Materials Research Express

**PAPER** • **OPEN ACCESS**

# Investigation on space charge dynamics and mechanical properties of Epoxy Alumina nanocomposites



To cite this article: Neelmani *et al* 2020 *Mater. Res. Express* **7** 025037



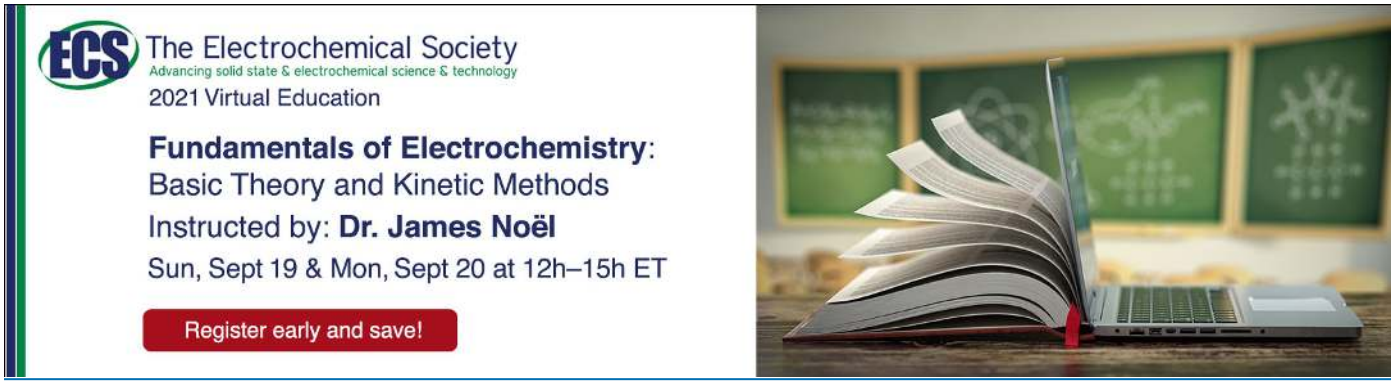

Materials Research Express

PAPER

# Investigation on space charge dynamics and mechanical properties of Epoxy Alumina nanocomposites

**Neelmani**[1], **Hisayuki Suematsu**[2] **and Ramanujam Sarathi**[1]

[1] Department of Electrical Engineering, IIT Madras, Chennai 600 036, India
[2] Extreme Energy-Density Research Institute, Nagaoka University of Technology, Nagaoka 940-2188, Japan

**E-mail:** rsarathi@iitm.ac.in

**Keywords:** nanocomposites, space charge, charge trap, dynamic mechanical analysis, surface potential, laser Induced breakdown spectroscopy, Pulsed Electro Acoustic technique

**OPEN ACCESS**

**RECEIVED**
8 October 2019

**REVISED**
21 November 2019

**ACCEPTED FOR PUBLICATION**
4 December 2019

**PUBLISHED**
17 February 2020



## Abstract

Epoxy nanocomposites with different wt% of alumina was prepared by use of high-speed shear mixer and high-frequency sonicator process, and the electrical and mechanical properties of the materials were investigated. Surface potential variation and trap distribution analysis were carried out with epoxy nanocomposites. Space charge analysis was carried out through Pulsed Electro Acoustic (PEA) technique. The dielectric constant and tan ($\delta$) values of epoxy alumina nanocomposites were measured at different frequencies and temperatures. Contact angle and corona inception voltage caused by a water droplet showed a direct correlation. The viscoelastic properties of the epoxy nanocomposite material were examined through DMA studies. It was concluded that an increase in the supply frequency increases the storage modulus and loss modulus of the epoxy alumina nanocomposites. Glass transition temperature and activation energy increase with an increase in wt% of alumina content in epoxy resin. LIBS analysis indicates that the plasma temperature calculated increases with an increase in the wt% of alumina content in epoxy resin. Also, the measured plasma temperature and hardness of the material showed a direct correlation.

## 1. Introduction

In recent times, epoxy resin has gained popularity as an insulant in dry-type transformer, GIS spacer, cable joints, etc [1]. With an increase in the power rating of the power equipment, it has become essential to design and develop a compact cost-effective and reliable insulating material. The improved high performance could be achieved by the use of suitable nano fillers with base material [2]. Earlier research has indicated that the addition of different types of nanoparticles (NP) to the base epoxy showed enhancement in dielectric strength, low dielectric loss with improved mechanical and thermal properties, and alumina nanoparticles emerged as some of the best nanofillers [1, 3].

In nanocomposites, the interface between the filler and base resin plays a vital role in influencing the dielectric properties of nanocomposites [4]. Under a high DC voltage, space charge can accumulate in the insulating material, which can cause local electric field enhancement, leading to early failure of insulation [5, 6]. The presence of any space charge in the insulating material during polarity reversal test is extremely dangerous and is one of the main causes for the failure of DC cables [6, 7]. It is indicated that an addition of nanoparticles to the insulating materials can suppress the space charge formation [8, 9]. Thus, an attempt is made, as a part of the study, to understand the space charge behaviour with epoxy alumina nanocomposites.

Surface flashover is a major threat to epoxy-based insulation structures [10]. Accumulation of charges on the surface of insulating material, over a period, can lead to surface discharge inception leading to surface flashover at the operating voltage [11]. Therefore, it is essential to understand the impact of charge accumulation on surface potential rise along with charge trap characteristics, with epoxy nanocomposite material.

In general, the polymeric insulating materials should be hydrophobic. The water droplet formed on the surface of the insulation structure due to fog condensation or due to rain, under normal operating voltage, can

create high electric field leading to surface discharge activity/tracking. Hence, it is essential to understand the performance of epoxy nanocomposites on water droplet initiated discharges.

The incipient discharges formed in insulation structures can be identified by the conventional partial discharge measurement studies [12]. In recent times, the ultra-high frequency (UHF) technique is gaining popularity because of its high sensitivity [13]. Thus, the inception of water-droplet-initiated discharges with epoxy nanocomposites need to be analysed by UHF technique.

In addition, the nanocomposite material should have good mechanical and thermal properties. Thus, the viscoelastic behaviour and hardness of the material were analysed by carrying out DMA studies and through Vickers hardness test on epoxy nanocomposites.

Laser-Induced Breakdown Spectroscopy (LIBS) is gaining considerable importance as a condition-monitoring technique. It can provide details of the elemental composition of the material, and can provide some correlation to its level of ageing. Aberkane *et al* have correlated plasma temperature calculated through LIBS and the hardness of the material [14].

Having known all these aspects, this study focuses on (i) variation in surface potential with epoxy nanocomposites with different wt% of alumina nanofiller (ii) characteristic variation in space charge accumulation and electric field variation in epoxy nanocomposites (iii) variation of dielectric constant and tan ($\delta$) of epoxy nanocomposites for different frequencies at different temperatures (iv) understanding the hydrophobicity and the variation in Corona Inception Voltage (CIV) caused by a water droplet on the epoxy nanocomposites (v) variation in the mechanical properties like storage modulus, loss modulus and hardness of the materials of epoxy nanocomposites (vi) LIBS analysis to correlate plasma temperature and the hardness of the material, in addition to composition analysis.

## 2. Experimental studies

### 2.1. Sample preparation

Epoxy resin (Araldite CY 205 IN Liquid, solvent-free, unmodified Bisphenol A epoxy resin purchased from HUNTSMAN) was used as a base material and alumina (size 20-30 nm, 99.9% purity from Richem international, USA) was used as a nanofiller. The nano alumina powder was dried at 150℃ for 24 h and then it was mixed with ethanol by sonication process. The sonicated mixture was added to epoxy resin. For complete mixing, shear mixing (for six hours at 4000 rpm) and high frequency sonication process (for one hour at 20 kHz) was adopted. Later the hardener (Tri-ethylene tetra-amine purchased from HUNTSMAN) of required ratio was added to epoxy-alumina mixture and degassed. The degassed mixture were poured in the mould of required dimension and left for curing at room temperature for 24 h by keeping them in a vacuum dessicator. Epoxy nanocomposites with 1, 3, and 5 wt% of alumina nanofiller were prepared. Before use of sample for any experiments, the samples were cleaned with ethanol and gently treated with hot air blower, to vapourise the ethanol and any surface moisture. Admittedly, further work need to be carried out to understand the impact of moisture on charge dynamics variation in epoxy alumina nanocomposites.

### 2.2. SEM analysis

Inspect F50 HRSEM Scanning Electron Microscope (SEM) was used to understand the uniform distribution of nano fillers in epoxy resin. Gold sputter coating was done for 120 s on each sample before examine the epoxy nanocomposites to get the better resolutions. SEM images were taken at the acceleration voltage of 20 kV, with different magnification.

### 2.3. Surface potential decay measurement

Figure 1 shows the experimental setup for surface potential measurement study. Needle-plane electrode configuration was used to deposit charges on surface of the insulating material (position 1) by generating corona at 10 kV DC voltage, for specific time and then moved to position 2 for surface potential variation. The studies were carried out with both polarity. The electrostatic voltmeter (Trek model 341B) was used to measure the surface potential.

### 2.4. Dielectric relaxation spectroscopy

Dielectric constant and dielectric losses of all samples were measured by Novo control technology broadband dielectric/impedance spectrometer (Alpha-A High performance frequency analyser). For the test, samples were cut into circular shape of 30 mm diameter and 1.5 mm thickness. Dielectric constant and dielectric loss were measured at different input signal frequency ranging from $10^{-1}$ to $10^{6}$ Hz.

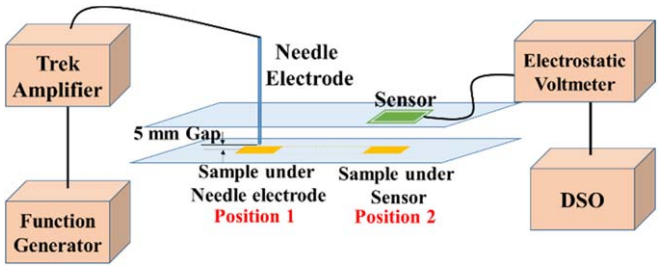


**Figure 1.** Experimental setup of surface potential decay measurement.

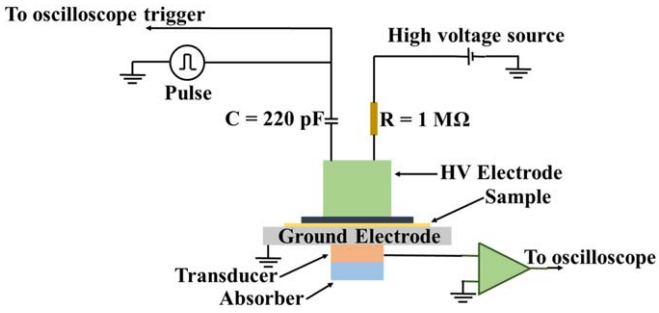


**Figure 2.** Schematic diagram of PEA setup for the space charge measurement.

### 2.5. Space charge measurement

For space charge measurement pulsed electro acoustic (PEA) technique is adopted. The PEA System consists of a PEA Flat cell, variable DC source of 0–30 kV, a pulse generator of 0–500 V, a DC power supply of 18–24 V for the amplifiers in the cell and an oscilloscope (Tektronix, 350 MHz, 5 GS $s^{-1}$). The test specimen used the study is with dimension of 40 × 40 × 1.5 mm. Figure 2 shows the schematic diagram of Techimp PEA setup. In the process of the measurement of space charge, poling voltage was applied for 1 h and then poling voltage was switched off so that all the space charge should get depleted, this process is known to be depoling. Depoling was done for 1 h for each sample.

In the present work, to know the effect of voltage reversal on space charge and electric field, voltage was reversed after 30 min of poling from positive to negative during the period of 30 s and continued poling for another 30 min in reverse polarity. After 1 h of poling and 30 s of reversal time, voltage was switched off and depoling was done for another 1 h.

### 2.6. Water droplet initiated discharge studies

Figure 3 shows the experimental setup for the measurement of in water droplet initiated corona discharge inception voltage (CIV). Two needle electrodes are kept at 45 degree each on the samples. Water droplet of 10 $\mu$l volume was put on the samples in between the two electrodes. One of the electrodes was given high voltage and other electrode was connected to ground. Input voltage was varied and corresponding CIV due to water droplet was characterised using UHF technique.

### 2.7. UHF technique

In the present work, a non-directional broad band sensor was used to sense the UHF signal produced during the discharge. Test cell was maintained at a distance of 15 cm from the UHF sensor. LeCroy digital real-time oscilloscope of sampling rate 10 GSa/s was used to capture UHF signal produced during the partial discharge.

### 2.8. Mechanical analysis

Dynamic mechanical analysis (DMA) was carried out by using NetzschDMA-242C through three point bending mode in the temperature range of 30–160 °C at the frequencies of 1, 10, and 50 Hz. Test was carried out with nanocomposites to know the viscoelastic behaviour by measuring storage modulus and loss modulus. The samples of dimension 50 × 12 × 1 mm was used for the DMA. Micro-Hardness test was performed on all the samples using 402MVD at a constant force of 980 mN with a dwell time 10 s. 10 readings were taken at different places for each sample and then it was averaged to obtain final hardness value.

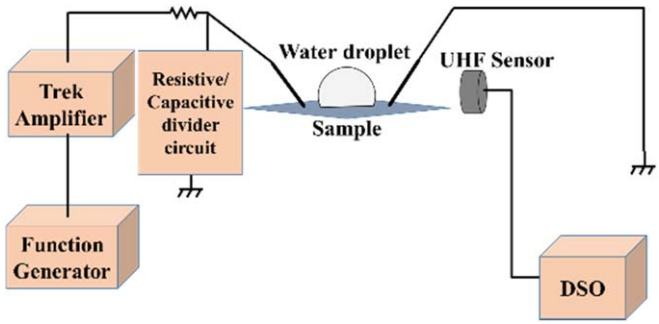


**Figure 3.** Experimental setup for measurement of CIV.

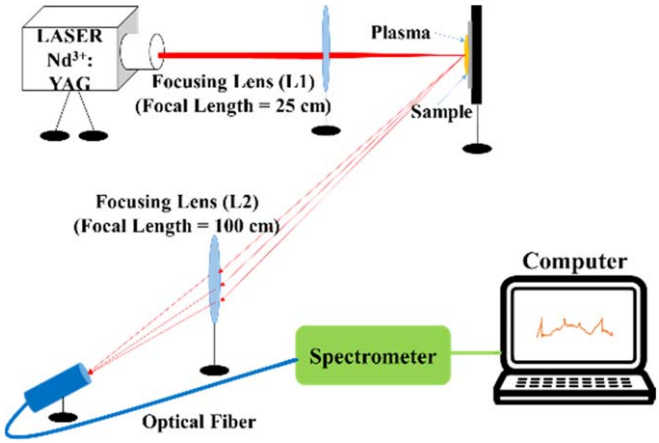


**Figure 4.** Experimental setup of Laser Induced Breakdown Spectroscopy.

### 2.9. Laser induced breakdown spectroscopy

Laser Induced Breakdown Spectroscopy (LIBS) was used to determine the elemental constituents of the nano composites. Plasma temperature was calculated using the spectra obtained after performing LIBS experiment. Figure 4 shows the experimental setup for LIBS studies. Nd3+: YAG laser (LAB-150–10-S2K) beam of pulse duration of approximately 10 nano seconds was used to shine the sample surface. Lens L1 was adjusted to focus the laser beam on the sample. As high energy laser is injected on the sample, plasma containing excited ions, neutral atoms, and electrons are induced. As plasma cools down and returns to lower energy states by releasing energy in the form of electromagnetic radiations. Focusing lens L2 was adjusted to capture these radiations and transfer it to spectrometer using optical fiber having a core diameter of 400 $\mu$m, with numerical aperture of 0.22. Integration period of 500 ms was set in order to capture the spectrum.

## 3. Results and discussion

### 3.1. SEM analysis

Figure 5 shows the SEM images of different wt% of nano alumina added epoxy nanocomposites. The images clearly indicates the uniform dispersibility of alumina nanofiller in the epoxy matrix. It was observed that nanoparticles were uniformly dispersed at lower wt% of nanoparticles. Agglomeration of alumina nanoparticles was observed in 5 wt% of alumina added epoxy nanocomposites.

### 3.2. Surface potential measurement and trap distribution analysis

Figure 6 shows the surface potential variation of epoxy nanocomposites with different wt% of alumina. The surface potential variation of epoxy nanocomposites, with respect to time can be approximated as exponential decay

$$V(t) = V_0 e^{-\lambda t} \quad (1)$$

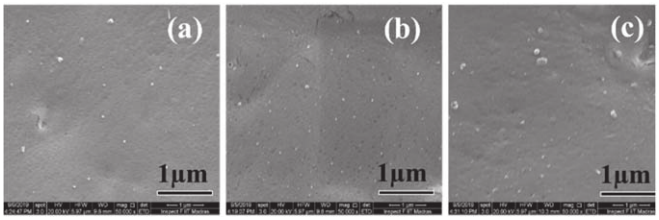


**Figure 5.** SEM images of alumina filled epoxy nanocomposites with (a) 1 wt%, (b) 3 wt%, (c) 5 wt% alumina nanofiller.

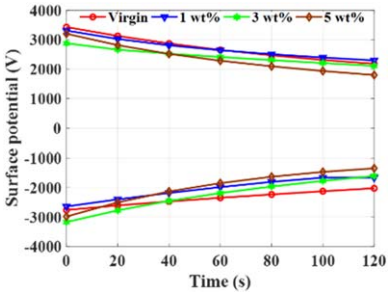


**Figure 6.** Surface potential decay characteristics for alumina filled epoxy nanocomposites.

**Table 1.** Variation of initial voltage and decay rate of pure epoxy and alumina filled epoxy nanocomposite under DC voltage.

| Sample | +DC | | | −DC | | |
|---|---|---|---|---|---|---|
| Wt% | Decay rate ($\lambda$) | Initial voltage ($V_o$) | Trap depth (eV) | Decay rate ($\lambda$) | Initial voltage ($V_o$) | Trap depth (eV) |
| 0 | 0.0063 | 3428 | 0.779 | 0.006 | −2761 | 0.787 |
| 1 | 0.0070 | 3311 | 0.763 | 0.0069 | −2642 | 0.782 |
| 3 | 0.0072 | 2879 | 0.763 | 0.0071 | −3170 | 0.773 |
| 5 | 0.0077 | 3203 | 0.751 | 0.0074 | −2984 | 0.768 |

where $V_o$ is the initial surface potential on the nanocomposites, $\lambda$ is the decay rate and $\tau = \frac{1}{\lambda}$ is the mean life time. The initial surface potential and decay rate of the epoxy nanocomposites on charging its surface under positive and negative DC corona are shown in table 1. This characteristic variation in charge decay process with nanocomposites could be due to surface charge de-trapping resistance performance on the addition of the alumina nanofiller. Du *et al* studied the effect of $TiO_2$ nanoparticles on the surface charge decay of epoxy and concluded that charge decay characteristics are highly dependent on the local surface states, that get altered on addition of nanoparticles. They also observed that surface potential decay faster in positive DC voltage as compared to negative DC voltage and also increases with the increase in the wt% of $TiO_2$ nanofiller [15]. Similar characteristics was observed in the present study.

According to isothermal current decay theory, the surface charge distribution can be obtained from surface potential characteristics. The distribution function of electrons or holes can be represented as [16].

$$N(E) = \frac{2\,\varepsilon_o \varepsilon_r}{qL^2 kTf_o(E)} t\frac{dV}{dt} \tag{2}$$

where $q$ is the electron charge, $L$ is thickness of sample, $k$ is Boltzmann constant, $T$ is absolute temperature, $t$ is time, and $f_o(E)$ is occupancy rate of initial electrons.

The trap depth $\Delta(E)$ can be expressed as

$$\Delta E = E_C - E_M = kT\,\ln(vt) \tag{3}$$

where $E_C$ is conduction band energy and $E_M$ trap level energy. Figure 7 shows variation in trap depth of epoxy alumina nanocomposites on charging its surface by corona ageing under positive DC and negative DC corona and it was observed that its value varied in the range of 0.71 to 0.83 eV. The trap depth at the peak value of trap distribution characteristics of epoxy nanocomposites under positive DC and negative DC corona were represented in table 1. A reduction in the trap depth can be observed due to left shift in the peak value of trap

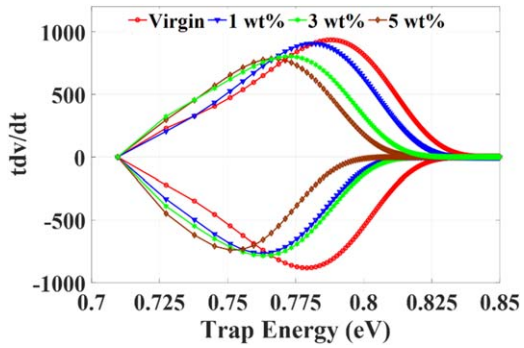


**Figure 7.** Trap distribution characteristics for alumina filled epoxy nanocomposites.

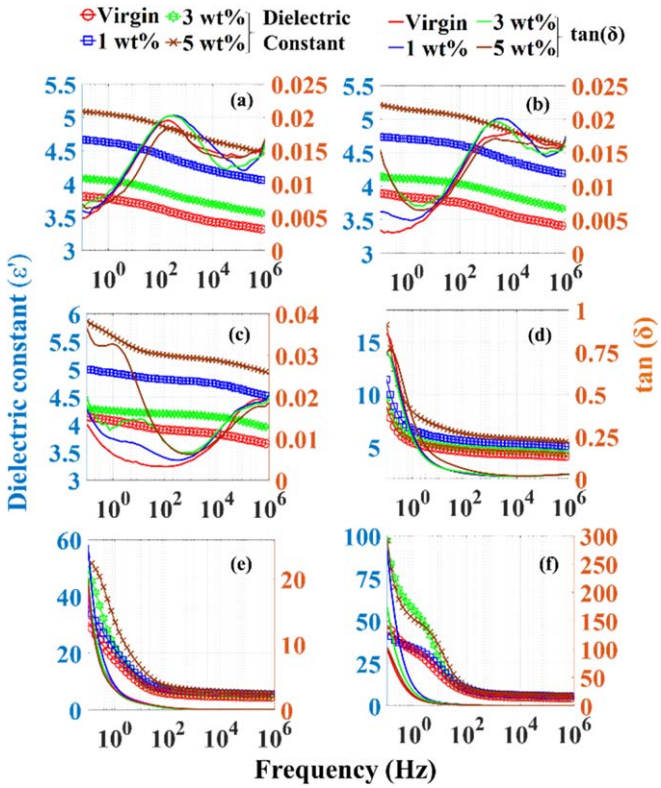


**Figure 8.** Variation in relative permittivity and tan ($\delta$) with the variation in frequency for alumina filled epoxy nanocomposites (a) −40° C, (b) −20° C, (c), 30° C, (d) 60° C, (e) 90° C and (f) 120° C.

distribution characteristics for increase in nano filler in epoxy nanocomposites. The high trap energy level means more number of deep traps in the composites which hinders the mobility of the trapped charge, as a result charge is getting captured into the deep trap which led to decrease in surface potential decay. This left shift in the peak value indicates the reduction of the energy barrier for charge detrapping. Thus, by correlating the surface potential decay rate with trap energy level, it shows inverse correlation.

### 3.3. Dielectric constant and loss tangent of nanocomposites

Figure 8 shows the variation in relative permittivity and tan ($\delta$) with the variation in supply voltage frequency at different temperatures. It was observed that dielectric constant of the epoxy nanocomposites filled with different wt% of alumina nanofiller had higher dielectric constant than that of virgin sample. Alumina nanofiller itself has high intrinsic permittivity value, as a result dielectric constant of epoxy nanocomposites increases on addition of the alumina nanofiller [17]. Dielectric constant decreased with the increase in the supply frequency. The properties of dielectric materials strongly depend upon the presence of dipoles and ions in the materials. At lower frequency of supply voltage, different functional group present in the sample orient along the direction of electric field, as a result higher permittivity was observed. On the other hand at higher frequency it is difficult for

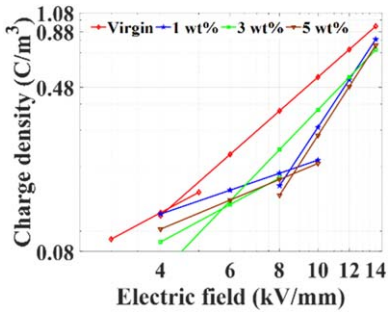


**Figure 9.** Field dependence of space charge density.

**Table 2.** Threshold electric field value for the space charge formed at the different applied electric field in all samples.

| Sample | Electric field (kV/mm) |
|---|---|
| Virgin | 4.17 |
| 1 wt% | 8.42 |
| 3 wt% | 5.69 |
| 5 wt% | 8.55 |

the induced dipoles to get synchronize and orient them along with the fast varying applied electric fields, thus causing reduction in permittivity value. It was observed that dielectric constant and tan ($\delta$) increases with the increase in the temperature. At lower temperatures, dipolar units from the epoxy are almost in frozen state, as temperature is increased, mobility of epoxy chain units started increasing and adding up to the existing dipoles, resulting in the increase in dielectric constant at higher temperature. At higher temperature above the glass transition temperature of composites, rapid increase in dielectric constant was observed as shown in figures 8(e) and 7(f). At the temperature above glass transition temperature abundant amount of charge carriers will be formed as a result of enhanced mobility of polymer chain segments, this charge carriers accumulated between the matrix and filler enhances the interfacial polarization effects which lead to increase in the dielectric constant. Variation of tan ($\delta$) at low temperature and at high temperature with the variation in frequency for different wt% of alumina filled epoxy nanocomposites was observed. Tan ($\delta$) increased with the increase in the alumina nanofiller content in the epoxy matrix and this enhancement was due to the increase in the charge carriers and variation in electrical conduction of charge carriers. At higher temperature, tan ($\delta$) value became significantly higher especially at lower frequencies range and this could be due to the increase in the electrical conductivity of thermally activated charge carriers [18].

### 3.4. Space charge analysis

*3.4.1. Space charge measurement*

Average amount of accumulated space charge density can be estimated using equation (4).

$$q_s(E,\ t) = \frac{1}{x_1 - x_0}\int_{x_0}^{x_1} Abs[q_p(x,\ t)]dx \tag{4}$$

where $x_0$ and $x_1$ are electrode positions (charges induced at the electrode are not taken into the consideration), E is the applied electric field, t is the poling and depoling time, and $Abs[q_p(x,\ t)]$ is the absolute value of the charge profile. Figure 9 shows the variation in space charge density with different applied electric field. It was observed an increase in space charge in sample with increase in applied electric field up to particular electric field and after that rapid increase in space charge was observed. This increase in space charge density clearly indicates the strong dependence of charge accumulation on the applied electric field. The electric field alone where significant increase in space charge accumulation was observed was called to be threshold electric field [19]. The value of threshold electric field of epoxy nanocomposites is tabulated in table 2. The value of threshold electric field is the highest for the 5 wt% sample.

For space charge studies during poling and depoling, analysis was carried out at an applied electric field of 10 kV mm$^{-1}$. Figure 10 shows the time dependent space charge profile during poling of epoxy nanocomposites under the electric field of 10 kV mm$^{-1}$. Heterocharges formation were observed in the vicinity of cathode was

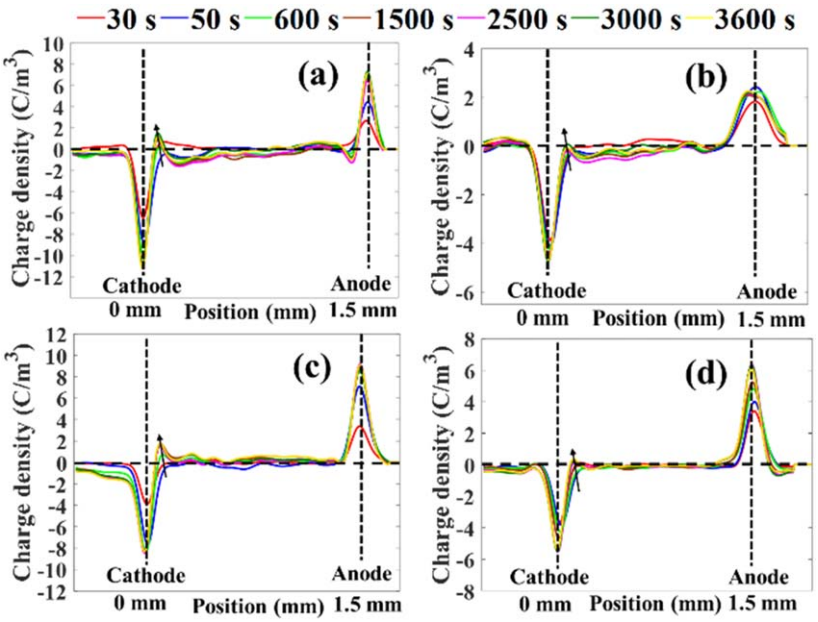


**Figure 10.** Time dependent space charge profile during poling under the electric field of 10 kV $mm^{-1}$ at the room temperature in (a) pure epoxy, (b) 1 wt%, (c) 3 wt%, (d) 5 wt% alumina filled epoxy nanocomposites.

**Table 3.** Space charge density in all the samples at the different electric field during 1 h of poling.

| Electric field (kV/mm) | Sample space charge density ($C/m^3$) | | | |
|---|---|---|---|---|
| | Virgin | 1 wt% | 3 wt% | 5 wt% |
| 4 | 0.081 | 0.073 | 0.054 | 0.058 |
| 6 | 0.122 | 0.112 | 0.097 | 0.101 |
| 8 | 0.143 | 0.128 | 0.115 | 0.124 |
| 10 | 0.464 | 0.14 | 0.280 | 0.132 |
| 12 | 0.505 | 0.434 | 0.387 | 0.395 |
| 14 | 0.586 | 0.51 | 0.458 | 0.480 |

due to the ionization of impurities present in the epoxy and due to the presence of dominant charge carrier, typically Na + ion in the epoxy resin [20]. At 3 wt% of alumina nanofiller, large heterocharges accumulation near the cathode were observed and at 5 wt% of nanofiller decrement of heterocharges were observed, and this could be due to the neutralization phenomenon happened near the cathode. Because of this neutralization phenomenon, decrement in inner electric field distribution after 2500 s was observed for 5 wt% alumina filled epoxy nanocomposites as shown in figure 14. Similar neutralization phenomenon was also reported by Qiang et al [21]. At 10 kV $mm^{-1}$ of electric field, space charge was minimum with 5 wt% of alumina added epoxy nanocomposites and pure epoxy sample had maximum space charge. Table 3 shows space charge density value for epoxy nanocomposites at different electric field and it clearly shows that space charge increased with the increase in the electric field. It was observed that sample with 3 wt% of nano alumina added epoxy resins accumulated less space charge at different electric except at 10 kV $mm^{-1}$, as shown in table 3, so performance of 3 wt% alumina added epoxy nanocomposites is better than the other samples. The evolution of space charge in the bulk of all the samples are shown in figure 11. Figure 12 shows the space charge decay profile during the 1 h of depoling period. Formation of heterocharges were observed in the samples. As the wt% of alumina nanofiller was increased, suppression in heterocharges were observed, and also decay of accumulated space charge became faster. Addition of nanofiller introduces a lot of shallow traps into the base epoxy, resulting into the enhancement in carrier mobility, as a result decay of space charge was high in the epoxy nanocomposites [22]. Figure 13 shows the variation of mean magnitude of space charge during poling and depoling in the bulk of pure epoxy and different wt% of alumina filled epoxy nanocomposites under the electric field of 10 kV $mm^{-1}$. Decay of the space charge formed in the bulk of nanocomposites on removal of applied electric field, can be approximated as exponential decay process.

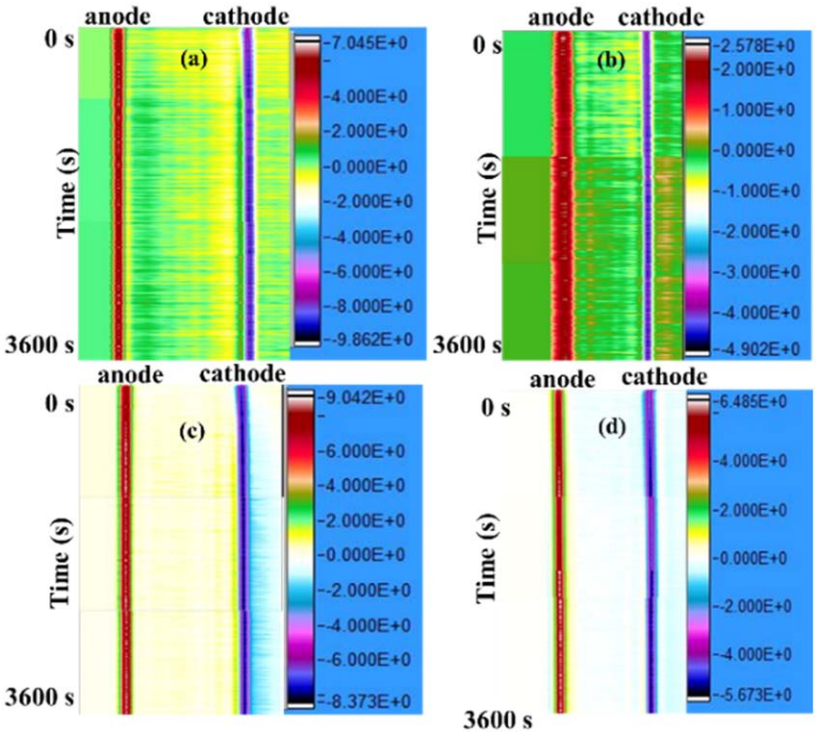


**Figure 11.** Space charge evolution under the electric field of 10 kV mm$^{-1}$ at the room temperature in (a) pure epoxy, (b) 1 wt%, (c) 3 wt%, (d) 5 wt% alumina filled epoxy nanocomposites.

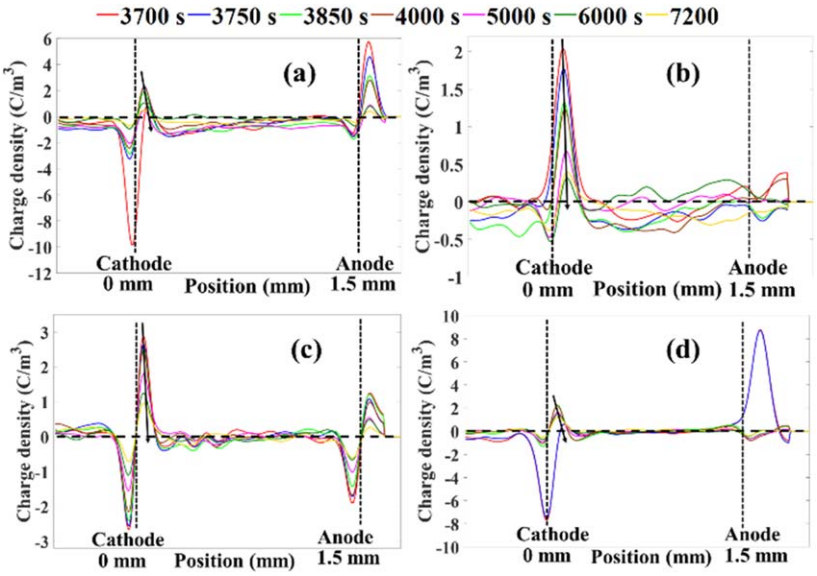


**Figure 12.** Space charge decay profile during depoling under the electric field of 10 kV mm$^{-1}$ at the room temperature in (a) pure epoxy, (b) 1 wt%, (c) 3 wt%, (d) 5 wt% alumina filled epoxy nanocomposites.

$$Q(t) = Q_{o} * e^{-\alpha t} \tag{5}$$

where $Q_o$ is the initial space charge and $\alpha$ is the decay rate. Table 4 shows the initial charge density and the decay rate of the space charge formed in the bulk of nanocomposites. Decay rate increased for the alumina filled epoxy nanocomposites.

Figure 14 shows the electric field distribution in pure epoxy and alumina filled epoxy nanocomposites under the application of 10 kV mm$^{-1}$. Field distortion near electrodes was observed in the pure epoxy due to formation of heterocharges near the electrodes. Enhancement in the electric field was also observed in the pure

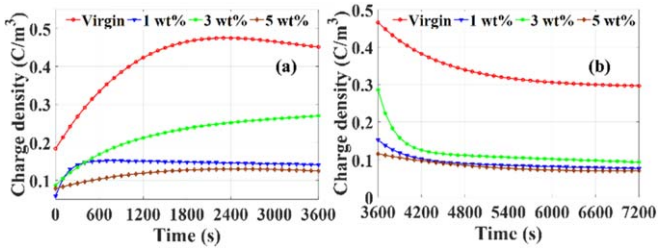


**Figure 13.** Space charge variation in pure epoxy and alumina filled epoxy nanocomposites under the electric field of 10 kV mm$^{-1}$ during (a) poling, (b) depoling period.

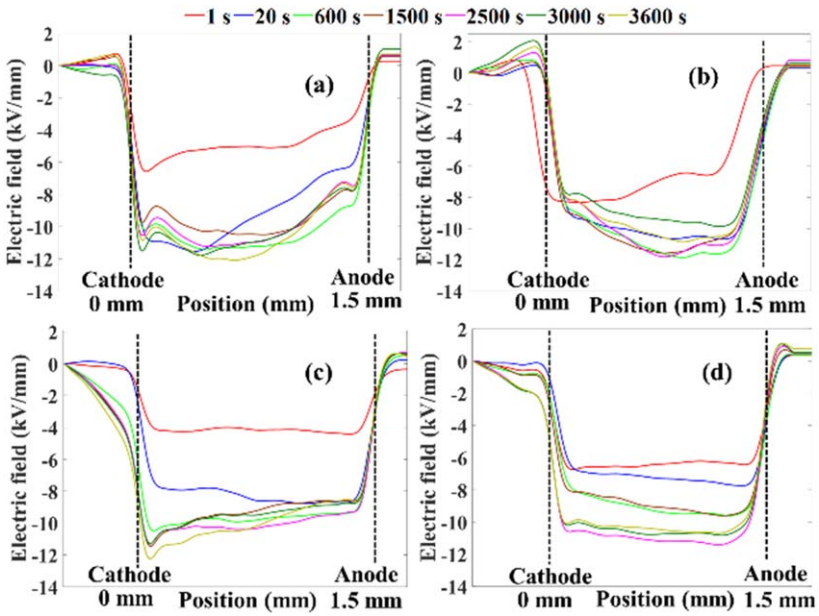


**Figure 14.** Electric field distribution under the electric field of 10 kV mm$^{-1}$ at room temperature in (a) pure epoxy, (b) 1 wt%, (c) 3 wt%, (d) 5 wt% alumina filled epoxy nanocomposites.

**Table 4.** Decay rate of the space charge formed at the 10 kV mm$^{-1}$ electric field in all samples.

| Sample | Initial space charge, $Q_o$ | Decay rate ($\alpha$) |
|---|---|---|
| Virgin | 0.4662 | 0.001294 |
| 1 wt% | 0.1533 | 0.002727 |
| 3 wt% | 0.2858 | 0.004742 |
| 5 wt% | 0.1159 | 0.003447 |

epoxy compared to the alumina filled epoxy nanocomposites and this was due to formation of more space charges.

*3.4.2. Effect of voltage polarity reversal on space charge and electric field*

Figures 15 and 16 respectively shows the variation in space charge distribution and electric field distribution in epoxy nanocomposites, with applied electric field of 14 kV mm$^{-1}$ and reversing its polarity from positive to negative in 30 s. In figures 15 and 16, the negative time indicates space charge distribution/electric field variation, the time before reversal of voltage polarity. Heterocharges were observed to form at cathode before reversal and these charges would be retained near cathode even after voltage reversal, resulting in the enhancement of electric field near cathode. At anode very less heterocharges were formed, as a result very less enhancement in electric field was observed [23]. Addition of alumina nanofiller to the epoxy resins suppressed

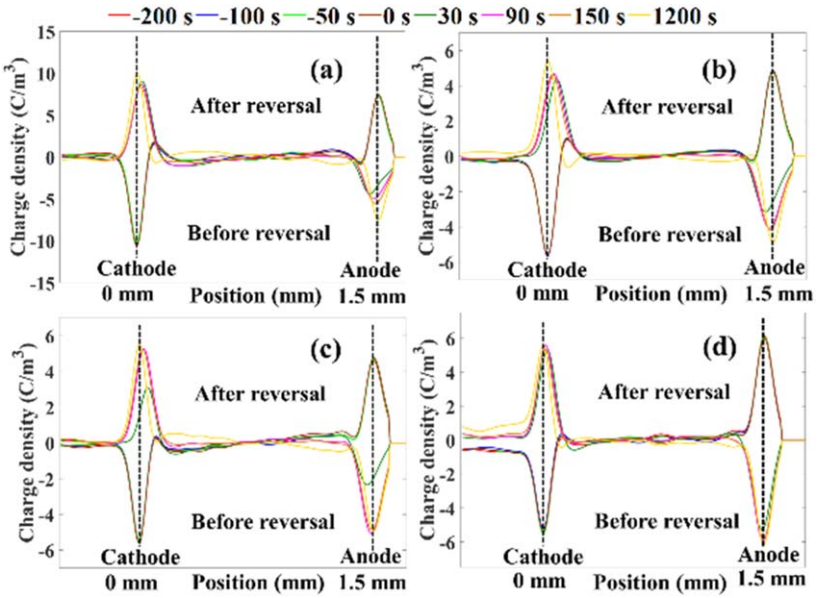


**Figure 15.** Space charge profile during poling under the electric field of 14 kV $mm^{-1}$ during the polarity reversal from positive to negative in (a) pure epoxy, (b) 1 wt%, (c) 3 wt%, (d) 5 wt% alumina filled epoxy nanocomposites.

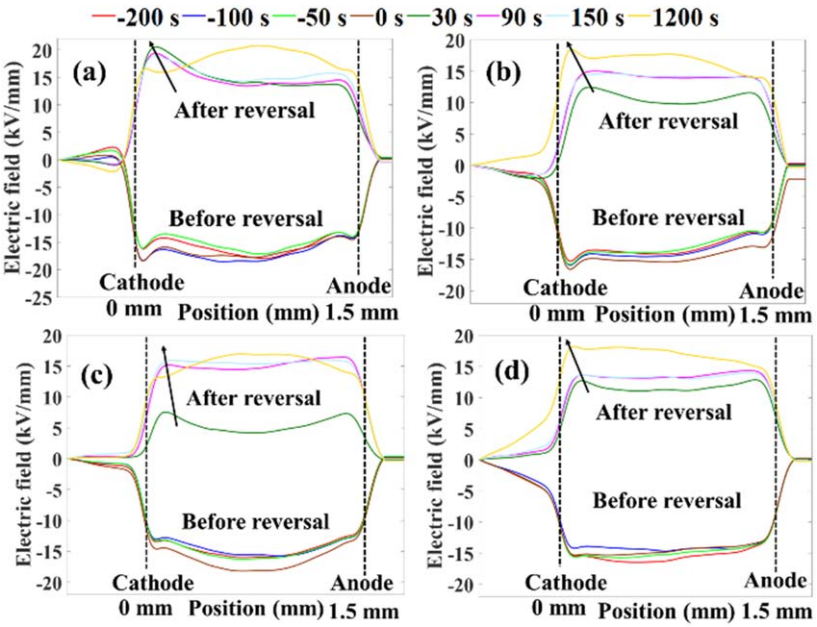


**Figure 16.** Electric field distribution under the electric field of 14 kV $mm^{-1}$ during the polarity reversal from positive to negative in (a) pure epoxy, (b) 1 wt%, (b) 3 wt%, (d) 5 wt% alumina filled epoxy nanocomposites.

the formation of space charge in the bulk, as a result less enhancement in electric field were observed in alumina filled epoxy nanocomposites compared to pure epoxy.

Field enhancement factor F was defined to know the extent of the field enhancement after voltage reversal, and can be written as

$$F = \frac{E - E_a}{E_a} \times 100 \tag{6}$$

where F is the field enhancement factor, E is the enhanced field after voltage reversal, and $E_a$ is the applied electric field. Field enhancement factor were calculated and tabulated in table 5 for all the samples, and it was found to be less for 3 wt% of alumina filled epoxy nanocomposites. Enhancement in electric field before and after the voltage reversal was observed, and difference was calculated, and tabulated in table 5. Field enhancement factor was calculated for 3 wt% of alumina filled epoxy nanocomposites on the application of different electric field and

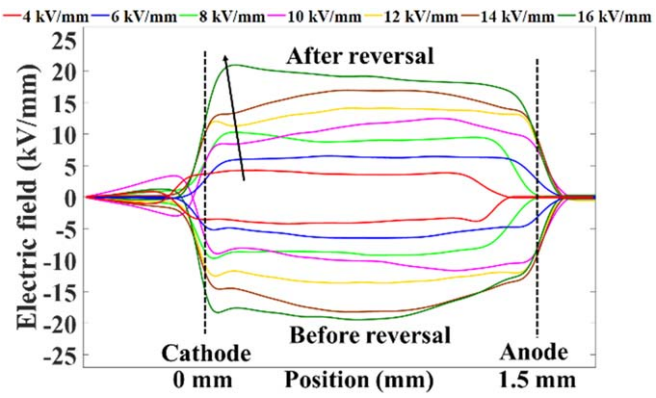


**Figure 17.** Electric field distribution in 3 wt% alumina filled epoxy nanocomposites under the application of different electric field during the polarity reversal from positive to negative.

**Table 5.** Field enhancement factor of virgin and alumina filled epoxy nanocomposites at 14 kV $mm^{-1}$ of electric field during the polarity reversal from positive to negative.

| Sample | Before reversal electric field (kV/mm) | After reversal electric field ($E_a$) (kV/mm) | Enhancement in electric field (kV/mm) | Field enhancement factor (F) |
|---|---|---|---|---|
| Virgin | 18.54 | 20.78 | 2.24 | 48.4 |
| 1 wt% | 16.56 | 18.45 | 1.89 | 31.78 |
| 3 wt% | 16.29 | 18.03 | 1.74 | 28.78 |
| 5 wt% | 16.45 | 18.21 | 1.76 | 30.07 |

**Table 6.** Field enhancement factor of 3 wt% alumina filled epoxy nanocomposites at different electric field during the polarity reversal from positive to negative.

| Applied Electric field (E) (kV/mm) | Before reversal electric field (kV/mm) | After reversal electric field ($E_a$) (kV/mm) | Enhancement in electric field (kV/mm) | Field enhancement factor (F) |
|---|---|---|---|---|
| 4 | 4.221 | 4.25 | 0.029 | 6.25 |
| 6 | 6.449 | 6.523 | 0.074 | 8.71 |
| 8 | 8.96 | 9.37 | 0.41 | 17.125 |
| 10 | 10.8 | 11.74 | 0.94 | 17.4 |
| 12 | 13.49 | 14.52 | 1.03 | 21 |
| 14 | 16.29 | 18.03 | 1.74 | 28.78 |
| 16 | 19.21 | 21.12 | 1.91 | 32 |

reversing its polarity from positive to negative in 30 s. Figure 17 shows the electric field distribution in 3 wt% sample on the application of different electric field during the voltage reversal from positive to negative and corresponding field enhancement factor were calculated and tabulated in table 6. Field enhancement factor increased drastically for the 3 wt% sample for the electric field above threshold value of field i.e. 5.69 kV $mm^{-1}$ and below this field, very less enhancement in electric field was observed.

### 3.5. Contact angle measurement and CIV

Hydrophobicity of nanocomposites were analyzed by measuring the water droplet static contact angle on the nanocomposites surface. Table 7 shows the measurement of static contact angle of alumina filled epoxy nanocomposites. It was observed that contact angle increased as the wt% of alumina nanofiller was increased. Table 8 shows the comparative variations in water droplet initiated corona discharge inception voltage on alumina filled epoxy nanocomposites surface under AC, + DC, - DC voltages. It was observed that CIV was very less on application of AC voltage as compared to DC voltages. This is due to variation in the shape of water droplet and conductivity of water droplet under AC and DC voltage profiles. CIV increased with the increase in wt% of alumina nanofiller and this increment is possibly due to increase in contact angle with the increase in wt% of alumina nanofiller. Water droplet was placed on the surface of sample in between the electrodes. As voltage was increased, water droplet started elongating along the axis of electrodes tip, as a result water droplet got sharpened at the tip, thereby enhancing the local electric field which lead to corona inception. High contact

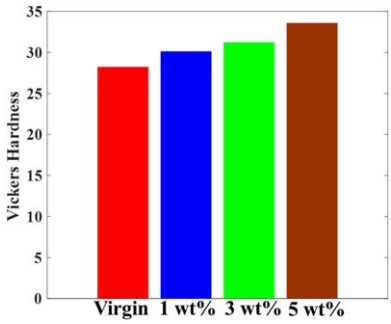


**Figure 18.** Vickers hardness value of the alumina filled epoxy nanocomposites.

**Table 7.** Contact angle measurement of alumina filled epoxy nanocomposites.

| Sample | Virgin | 1 wt% | 3 wt% | 5 wt% |
|---|---|---|---|---|
| Contact angle | 65.32° | 70.22° | 72.66° | 75.70° |

**Table 8.** Variation in CIV of alumina filled epoxy nanocomposites under (a) AC, (b) + DC and (c) –DC voltage.

| Sample | CIV (kV) | | |
|---|---|---|---|
| | AC | +DC | −DC |
| Virgin | 0.709 | 1.1825 | 1.05 |
| 1 wt% | 0.773 | 1.3945 | 1.23 |
| 3 wt% | 0.832 | 1.412 | 1.3 |
| 5 wt% | 0.882 | 1.485 | 1.375 |

angle means water droplet can't spread over the surface of sample thereby increasing the distance between droplet and electrodes, as a result inception due to water droplet occurred at higher voltage.

### 3.6. Mechanical properties of alumina added epoxy nanocomposite

*3.6.1. Hardness test*

Figure 18 shows the variation in hardness with different wt% of nano alumina added epoxy nanocomposites. It was observed that hardness value increased with the increase in wt% of alumina nanofiller. Hardness is actually the ability of material to resist from deformation and penetration on application of force. Alumina is itself a hard ceramic materials that is one of the reason for increment in hardness of material. As indenter applies force on the surface of materials, pressure developed on the surface should be transmitted efficiently in order to resist from any indentation. Uniformly dispersed nanoparticles transmit the pressure more efficiently, as a result very less indentation was observed on the surface of samples with alumina nanoparticles thereby increasing the hardness value.

*3.6.2. Dynamic mechanical analysis*

The viscoelastic properties of alumina-epoxy nanocomposites were evaluated using Dynamic mechanical analysis. Figure 19 shows the variation of storage modulus and tan ($\delta$) for 1 wt% alumina included epoxy nanocomposites with the variation of temperature at different frequency of applied force. It was observed that storage modulus and tan ($\delta$) increased with increase in frequency. The peak of tan ($\delta$) in the range of temperature studied is identified as glass transition temperature ($T_g$). For different frequencies, the glass transition temperature was observed to be varying. Storage modulus of materials starts decreasing once it reaches glass transition phase.

Figure 20 shows the variation of storage modulus and tan ($\delta$) with the variation of temperatures for the epoxy nanocomposites with different wt% of nano alumina. It was observed that storage modulus increased with the increase in wt% of alumina in epoxy nanocomposites. At higher wt% of alumina nanofiller, a marginal

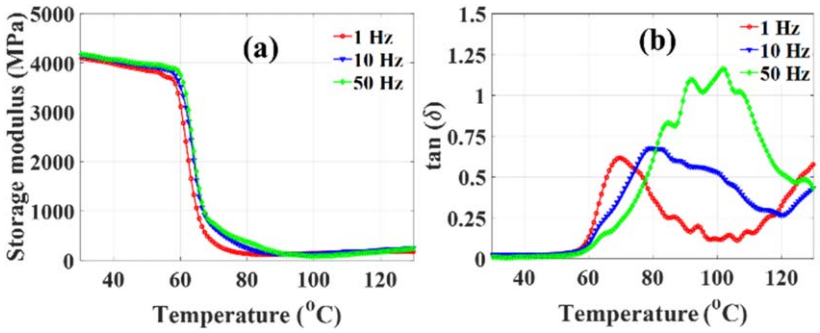


**Figure 19.** Dynamic mechanical analysis of 1 wt% alumina filled epoxy nanocomposites (a) Storage modulus, (b) tan ($\delta$).

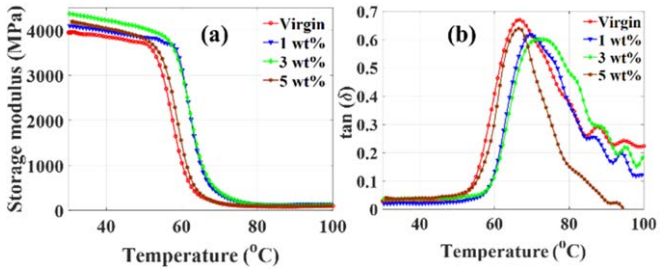


**Figure 20.** Dynamic analysis of alumina filled epoxy nanocomposites with different wt% of alumina nanofiller (a) Storage modulus, (b) tan ($\delta$).

reduction in storage modulus was observed which could be due to the agglomeration of nanofiller. Figure 20(b) shows the variation in tan ($\delta$) with the variation of temperature. It was observed that glass transition

peaks decreased and shifted towards right on the addition of alumina nanoparticles and the cause for it could be due to reduction in the mobility of polymer chains on addition of nanoparticles to the epoxy resins [24]. Decrease in the transition peaks on addition of nanoparticles implies a reduction in viscoelastic nature of the nanocomposites and interfacial losses, indicating interfacial bonding between the epoxy matrix and alumina nanofiller enhanced. This enhancement in interfacial bonding lead to increment in $T_g$ value with the increase in wt% of alumina nanofiller but at 5 wt% of nanofiller, decrement in $T_g$ was observed due to agglomeration of alumina nanoparticles in epoxy resins.

Activation energy is the minimum energy required to start any structural changes inside the materials. Activation energy of the samples were determined using Arrhenius equation.

$$f = f_0 \exp\left[\frac{-E_a}{RT}\right] \tag{7}$$

$$\ln f = \ln f_o - \frac{E_a}{RT} \tag{8}$$

where f is the frequency of input signal, $f_o$ is a proportionality constant, $E_a$ is the activation energy, R is gas constant, T is temperature. Figure 21 shows the linear relationship between the frequency and glass transition temperature. The slope of the graph provides the activation energy and is tabulated in table 9. Activation energy increases with the increase in wt% of alumina in epoxy nanocomposites.

### 3.7. LIBS analysis

Figure 22 shows the LIBS spectrum of alumina filled epoxy nanocomposites. LIBS was carried out for characterizing the constituent elements of materials. Aluminium (Al) (both neutral and ionic form) peaks was observed on all the samples except pure epoxy sample. Carbon (C), Oxygen (O), and Nitrogen (N) were main constituents of all samples. In the LIBS experiment, laser beam is injected on the surface of sample as a result, plasma is produced due to the ablation of materials. The plasma temperature can be calculated using Boltzmann-Saha equation [25].

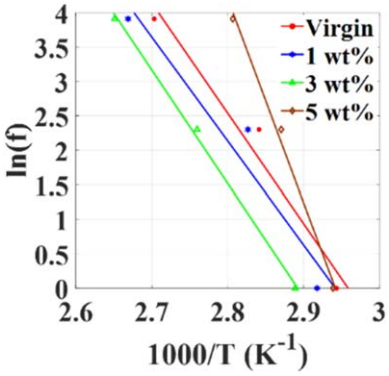


**Figure 21.** Activation energy calculation of alumina filled epoxy nanocomposites.

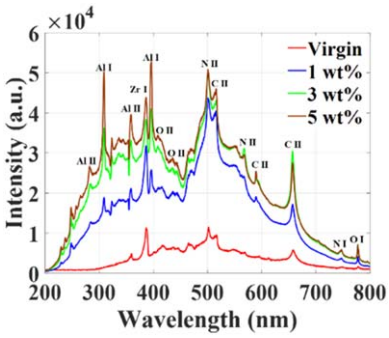


**Figure 22.** LIBS spectrum of alumina filled epoxy nanocomposites.

**Table 9.** Calculated mechanical parameters of alumina filled epoxy nanocomposites.

| Sample | Activation energy (kJ/mol) | $T_g$ (°C) | Plasma temperature (K) |
|---|---|---|---|
| Virgin | 16.038 | 80.88 | 125924 |
| 1 wt% | 16.212 | 84.07 | 140974 |
| 3 wt% | 16.493 | 88.90 | 147265 |
| 5 wt% | 29.70 | 82.13 | 156976 |

$$T_e = 1.44 \frac{E_2 - E_1}{\ln\left[\frac{I_1 \lambda_1 A_2 g_2}{I_2 \lambda_2 A_1 g_1}\right]} \quad (9)$$

where $E_1$ and $E_2$ are excited energy levels, $I_1$ and $I_2$ are intensities of corresponding atomic species at wave lengths $\lambda_1$ and $\lambda_2$, $A_1$ and $A_2$ represents transition probabilities of energy states, $g_1$ and $g_2$ are the statistical weights of corresponding excited energy levels, and $T_e$ is the plasma electron temperature at the local thermodynamic equilibrium. Table 9 shows the plasma temperature of all the samples. Plasma temperature was calculated using the spectral line of O I and O II. It was observed that plasma temperature was low for the virgin sample and it increased on increasing the wt% of alumina nanoparticles. Further surface degradation was analysed of all the samples by forming crater using laser pulses. 20 number of pulses of equal energy were hit on the surface of all the samples to form crater on the surface of samples. Figure 23(a) shows the variation in crater depth with the variation of alumina nanofiller. It was observed that crater depth decreases with the increase of wt% of nanofiller. Figure 23(b) shows the typical 3D image of the crater created by the laser pulses.

## 4. Conclusions

The important conclusions derived, based on the present study, are the following

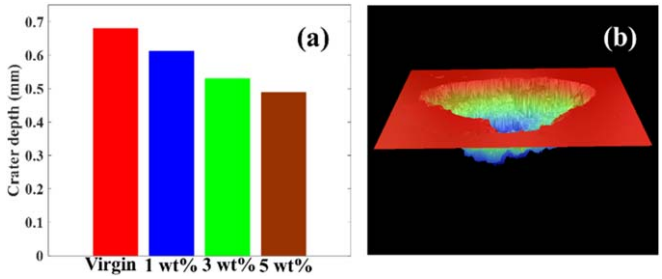


**Figure 23.** Crater depth variation and crater image (a) Variation in crater depth of alumina added epoxy nanocomposites, (b) Typical 3D image of crater.

- Surface potential decay measurement indicates that the decay rate increased with an increase in the wt% of alumina in epoxy resin. Trap distribution analysis indicates a reduction in trap energy with the increase in wt% of nano alumina in epoxy resin.
- Space charge accumulation and electric field distortion factor measured during polarity reversal test were found to be less with the addition of alumina nano filler of up to 3 wt% in epoxy resin.
- Dielectric constant and tan ($\delta$) values of epoxy alumina nanocomposites are different at low and high temperatures. Also, the supply voltage frequency has a huge impact on its variations.
- Contact angle increases with an increase in the wt% of alumina nanofiller in epoxy resin. The voltage at which corona incepts due to water droplet, under AC voltage, was identified adopting the UHF technique. The corona inception voltage and the contact angle showed a direct correlation.
- DMA results indicate that the storage modulus increases and loss modulus decreases with an increase in the wt% of alumina nanofiller. It was observed that an increase in the supply frequency showed an increase in the storage modulus and loss modulus of the epoxy alumina nanocomposites. Glass transition temperature and activation energy measured showed an increasing trend with an increase in the wt% of alumina content in epoxy resin.
- Vickers hardness value increased with an addition of alumina nanofiller to the base epoxy.
- LIBS analysis indicated that the plasma temperature increases with an increase in the wt% of alumina content in epoxy resin. Also, the measured plasma temperature and hardness of the material show a direct correlation.

## Acknowledgments

The Author (R.S) wish to thank Department of Science and Technology, New Delhi for sponsoring the project (DST/NM/NT/2018/33(c)) on nanocomposites. Also would like to thank Central power research institute, Bangalore for their support to use the PEA equipment acquired from the project sponsored by them.

## ORCID iDs

Neelmani https://orcid.org/0000-0002-2829-4720
Ramanujam Sarathi https://orcid.org/0000-0002-1353-9588

## References

[1] Tanaka T, Montanari G C and Mulhaupt R 2004 Polymer nanocomposites as dielectrics and electrical insulation-perspectives for processing technologies, material characterization and future applications *IEEE Trans. Dielectr. Electr. Insul.* **11** 763–84
[2] Tanaka T and Imai T 2017 *Advanced Nanodielectrics: Fundamentals and Applications* (United States of America: CRC Press)
[3] Maity P, Poovamma P K, Basu S, Parameswaran V and Gupta N 2009 Dielectric spectroscopy of epoxy resin with and without nanometric alumina fillers *IEEE Trans. Dielectr. Electr. Insul.* **16** 1481–8
[4] Todd M G and Shi F G 2003 Molecular basis of the interphase dielectric properties of microelectronic and optoelectronic packaging materials *IEEE Trans. Components Packag. Technol.* **26** 667–72
[5] Li Y and Takada T 1992 Experimental observation of charge transport and injection in XLPE at polarity reversal *J. Phys. D: Appl. Phys.* **25** 704–16
[6] Zhang Y, Lewiner J, Alquie C and Hampton N 1996 Evidence of strong correlation between space-charge buildup and breakdown in cable insulation *IEEE Trans. Dielectr. Electr. Insul.* **3** 778–83

[7] Fu M, Dissado L A, Chen G and Fothergill J C 2008 Space charge formation and its modified electric field under applied voltage reversal and temperature gradient in XLPE cable *IEEE Trans. Dielectr. Electr. Insul.* **15** 851–60
[8] Tian F Q, Lei Q Q, Wang X and Wang Y 2011 Effect of deep trapping states on space charge suppression in polyethylene/ZnO nanocomposite *Appl. Phys. Lett.* **99** 14
[9] Takada T, Hayase Y, Tanaka Y and Okamoto T 2008 Space charge trapping in electrical potential well caused by permanent and induced dipoles for LDPE/MgO nanocomposite *IEEE Trans. Dielectr. Electr. Insul.* **15** 152–60
[10] Yu S, Li S, Wang S, Huang Y, Nazir M T and Phung B T 2018 Surface flashover properties of epoxy based nanocomposites containing functionalized nano-$TiO_2$ *IEEE Trans. Dielectr. Electr. Insul.* **25** 1567–76
[11] Miller H C 1989 Surface flashover of insulators - Electrical Insulation *IEEE Trans. Electr. Insul.* **24** 765–86
[12] IEC Std 2000 60270 High Voltage Test Techniques—Partial Discharge Measurements
[13] Judd M D and Farish O 1998 A pulsed GTEM system for UHF sensor calibration *IEEE Trans. Instrumentation Measurement* **47** 875–80
[14] Aberkane S M, Bendib A, Yahiaoui K, Boudjemai S, Messaci S A, Kerdja T, Amara S E and Harith M A 2014 Correlation between Fe–V–C alloys surface hardness and plasma temperature via LIBS technique *Appl. Surf. Sci.* **301** 225–9
[15] Du B X, Zhang J W and Gao Y 2012 Effects of $TiO_2$ particles on surface charge of epoxy nanocomposites *IEEE Trans. Dielectr. Electr. Insul.* **19** 755–62
[16] Simmons J G and Tam M C 1973 Theory of isothermal currents and the direct determination of trap parameters in semiconductors and insulators containing arbitrary trap distributions *Phys. Rev.* B **7** 3706–13
[17] Lide D R 1999 *CRC Handbook of Chemistry and Physics* (Florida United States of America: CRC Press)
[18] Katayama J, Ohki Y, Fuse N, Kozako M and Tanaka T Effects of nanofiller materials on the dielectric properties of epoxy nanocomposites *IEEE Trans. Dielectr. Electr. Insul.* **20** 157–65
[19] Montanari G C and Fabiani D 2000 Evaluation of dc insulation performance based on space-charge measurements and accelerated life tests *IEEE Trans. Dielectr. Electr. Insul.* **7** 322–8
[20] Ulaski J, Friedrich K and Boiteux G 1997 Evolution of ion mobility in cured epoxy-amine system as determined by time-of-flight method *J. Appl. Polym. Sci.* **65** 1143–50
[21] Qiang D, Wang Y, Wang X, Chen G and Andritsch T 2019 The effect of filler loading ratios and moisture on DC conductivity and space charge behaviour of $SiO_2$ and hBN filled epoxy nanocomposites *J. Phys. D: Appl. Phys.* **52** 395502
[22] Fabiani D, Montanari G C, Dardano A, Guastavino G, Testa L and Sangermano M 2008 Space Charge Dynamics in Nanostructured Epoxy Resin *Conf. on Electrical Insulation and Dielectric Phenomena*
[23] Chen X, Wang X, Wu K, Peng Z R, Cheng Y H and Tu D M 2012 Effect of voltage reversal on space charge and transient field in LDPE films under temperature gradient *IEEE Trans. Dielectr. Electr. Insul.* **19** 140–9
[24] Goyanes S N, Konig P G and Marconi J D 2003 Dynamic mechanical analysis of particulate-filled epoxy resin *J. Appl. Polym. Sci.* **88** 883–92
[25] Atwee T, Aschke L and Kunze H J 2000 Investigations of laser-produced plasmas from boron nitride targets *J. Phys. D: Appl. Phys.* **33** 2263–7